UVSOR

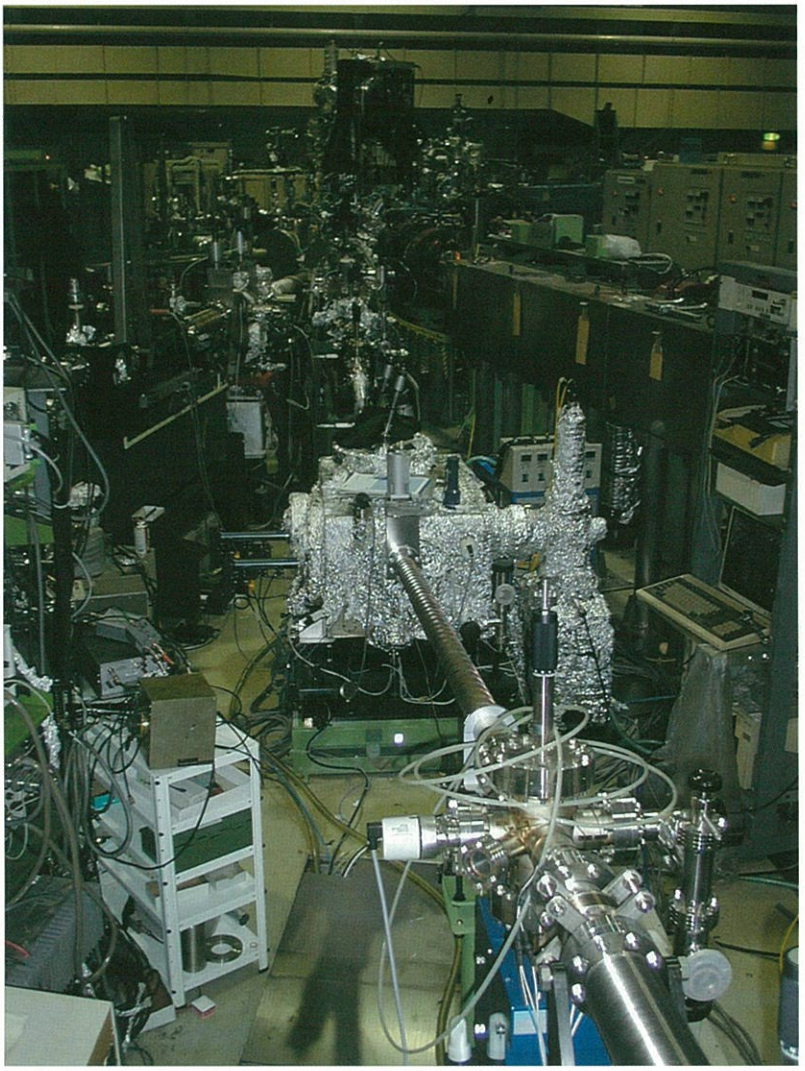

Instrumental Developments

Measurement of nonlinear momentum compaction factor in the UVSOR storage ring

Masahito HOSAKA, Jun-ichiro YAMAZAKI, Shigeru KODA and Hiroyuki HAMA
UVSOR Facility, Institute for Molecular Science, Okazaki 444-8585, Japan
Hitoshi TANAKA
Spring-8, Mikazuki, Sayo-gun, Hyogo 679-5198, Japan

There is a growing interest in operating of ring accelerator with extremely low momentum compaction factor. Such low momentum compaction factor, if attained, would lead to short bunched-beam that can be used for the generation of coherent radiation, and an isochronous condition that enables high power storage ring free electron laser. On the UVSOR storage ring, we have succeeded to operate the ring with momentum compaction factor reduced to one hundredth of the ordinal value by changing the dispersion function [1]. In the study we have found that nonlinear terms are serious problem to reduce momentum compaction factor further and precious study on them is needed, however there was no exact theoretical approach on them. Only recently Tanaka et al. have formulated a nonlinear dispersion function in storage ring and developed a code which gives higher order terms up to the fifth order [2]. In order to proceed with the study we have performed an experiment to observe the nonlinear behavior of momentum compaction factor and compared the result with the theoretical calculations.

The momentum compaction factors $\alpha_1, \alpha_2, \alpha_3, \ldots$ connect the momentum deviation dp/p to the fractional elongation $\Delta l/l$ as

$$\Delta l / l = \alpha_1 (\Delta p / p) + \alpha_2 (\Delta p / p)^2 + \alpha_3 (\Delta p / p)^2 + \ldots . \tag{1}$$

Then a local value of the momentum compaction factor at a momentum deviation of dp/p can be written as

$$\alpha_{Local}(\Delta p / p) = \frac{d(\Delta l / l)}{d(\Delta p / p)} = \alpha_1 + 2\alpha_2 (\Delta p / p) + 3\alpha_3 (\Delta p / p)^2 + \ldots, \tag{2}$$

and the synchrotron oscillation frequency is given as

$$f_s = \frac{1}{2\pi}\sqrt{\frac{e\dot{V}_{RF}}{TE}\alpha_{Local}} = \frac{1}{2\pi}\sqrt{\frac{e\dot{V}_{RF}}{TE}\left[\alpha_1 + 2\alpha_2 (\Delta p / p) + 3\alpha_3 (\Delta p / p)^2 + \ldots\right]}, \tag{3}$$

where e, $\dot{V}_{RF}$, T and E are the electron charge, the slope of the RF field, the revolution time and the electron energy, respectively. Thus the nonlinear behavior of the momentum compaction factor can be investigated by measuring the synchrotron oscillation frequency as a function of the momentum deviation.

The experiment was carried out at the electron energy of 600 MeV, which is the maximum energy of the synchrotron and at the operation points of both positive and negative linear momentum compaction factor [3]. The synchrotron oscillation frequency was deduced through the collective synchrotron oscillation excited due to beam instability. We varied the RF frequency from the central value step by step until the acceptance limit and measured the synchrotron frequency as a function of the RF frequency. We also varied excitation current of focusing sextupole magnets in order to derive the dependence on sextupole strength. In Fig. 1, the experimental local momentum compaction factor (α_{Local}) deduced using Eq. (3) as a function of the deviation of the RF frequency is shown. As seen in the figure, nonlinear behavior due to the higher order momentum compaction factors ($\alpha_2, \alpha_3, \ldots$) is clearly observed. The central RF frequency ($\Delta f / f = 0$) in the figure was derived from the cross point that is independent of the value of the sextupole strength. This means that in the central RF frequency the electron beam passes through the averaged magnetic center of the sextupole magnets. The calculated local momentum compaction factor using the code [2] is also shown by the solid line in the figure. In the calculation, we have taken into account the higher order terms up to the fifth order (the maximum order obtained in the calculation code) and made a correspondence between the deviation of momentum and RF frequency as

$$\Delta f / f = -\left[\alpha_1 + \alpha_2(\Delta p / p) + \alpha_3(\Delta p / p)^2 + \alpha_4(\Delta p / p)^3 + \alpha_5(\Delta p / p)^4\right](\Delta p / p). \quad (4)$$

As seen in the figure, the calculated local momentum compaction factor agrees well with the experimental value. In order to confirm significance of the higher order terms of momentum compaction factor, we changed the maximum order of α included in the calculation and compared each value with the experimental ones. In the comparison, we found that up to the third order the calculation comes closer to the experiment as the maximum order increases, but on the calculation up to the forth order no actual improvement can be observed. This indicates that the contribution from more than the forth order terms is small and is obscured by the experimental errors. We think that source of the error comes from the incomplete modeling of the magnetic strength and the closed orbit distortion.

In this work, we have shown validity of the formalism by Tanaka et. al. up to the third order terms. More accurate study is needed to investigate further higher order terms and we are proceeding with it.

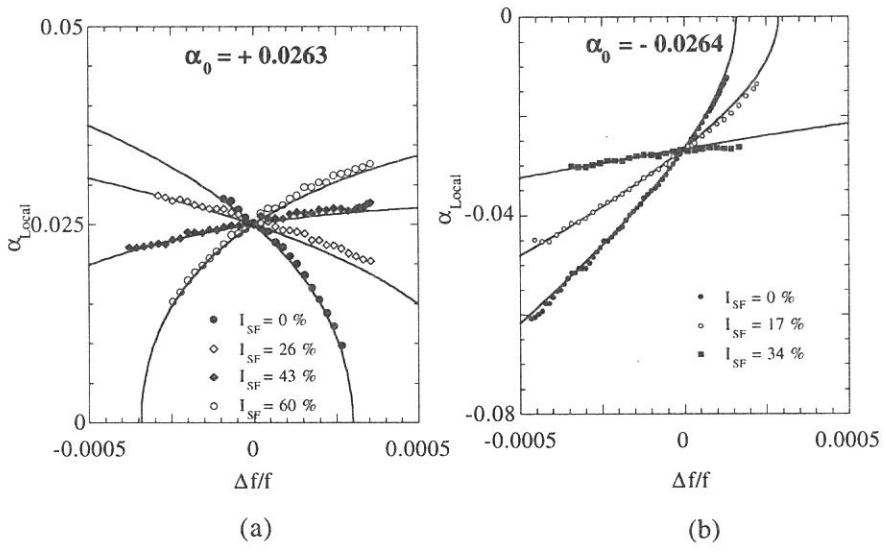

Figure 1. Variation of the local momentum compaction factor versus RF frequency for different sets of sextupoles , for positive (a) and negative first order momentum compaction factor. The solid line shows the calculated value.

References

[1] H. Hama et. al. Nucl. Instr. and Meth. A 329 (1993) 29.

[2] H. Tanaka et. al. Nucl. Instr. and Meth. A 431 (1999) 369.

[3] M. Hosaka et. al. Nucl. Instr. and Meth. A 407 (1998) 234.

(BL2B1)

Development of a new electron-ion coincidence analyzer

Kazuhiko Mase, Shin-ichiro Tanaka,[A] Eiji Ikenaga,[B] Kenichiro Tanaka,[B] Tsuneo Urisu[C]

Photon Factory, Institute of Materials Structure Science, High Energy Accelerator Research Organization, 1-1 Oho, Tsukuba 305-0801, [A]Department of Physics, Graduate School of Science, Nagoya University, Chikusa-ku, Nagoya 464-8602, [B]Department of Physics Science, Faculty of Science, Hiroshima University, Higashi-Hiroshima 739-8527, [C]Institute for Molecular Science, Okazaki 444-8585

Energy-selected electron ion coincidence (EICO) spectroscopy is an ideal tool for investigations of the ion desorption induced by electronic transitions, because it provides ion mass spectra for the ion desorption channels related to the selected electron transitions [1]. We have developed the first EICO apparatus combined with synchrotron radiation for the study of surface dynamics in 1996 [2]. A remodeled EICO analyzer was developed in 1998 the sensitivity of which was improved by the factor of 5 as compared with the second one [1]. In the present article, we describe the third EICO analyzer developed recently [3]. Every EICO analyzer was constructed on a 203-mm-diameter conflat flange as a bolt-on instrument, which consists of a cylindrical mirror analyzer (CMA) for detection of energy-resolved electrons, a time-of-flight ion mass spectrometer (TOF-MS) for ion detection and a retraction mechanism. Since the signal-to-background ratio of coincidence spectroscopy is linearly dependent on the collection efficiency of electrons and ions, the solid angles of CMA and TOF-MS were improved at every remodeling. Figure 1 shows a schematic diagram of the third EICO apparatus. In order to achieve a fair signal-to-background ratio within a reasonable data collection time, the solid angle of the CMA is designed to be 1.1 sr. The TOF-MS without a deflector is located coaxially with the CMA. With these reforms the signal-to-background ratio was improved by a factor of 5 as compared with the second one. The resolving power of the CMA was limited to $E/\Delta E = 100$ because of the large solid angle, the relatively large spot size of synchrotron radiation (1×1 mm^2) and ion extraction field (17 V/mm). The ion detection efficiency of the TOF-MS is 0.4. The EICO analyzer was attached to an ultrahigh vacuum chamber at the BL-2B1. The surface normal was set coaxial to the CMA and TOF-MS. A sample surface was excited by *p*-polarized radiation with an incident angle of 60° , and the emitted electrons were energy-selected and detected by the CMA, while the desorbed ions were mass-analyzed and detected by the TOF-MS. The ion counts were recorded as a function of the TOF difference between the energy-selected electron and the ion with a multi channel scaler (MCS) by taking the electron signal as the starting trigger. The ion desorbed in coincidence with the detected electron gives a coincidence signal at a specific TOF, while the ion irrelevant to the electron increases the background level. Since the selected electron kinetic energy corresponds to particular photoemission or Auger transitions, the coincidence signal intensity offers the yield of the ion desorption induced by the selected core-excitations or Auger transitions.

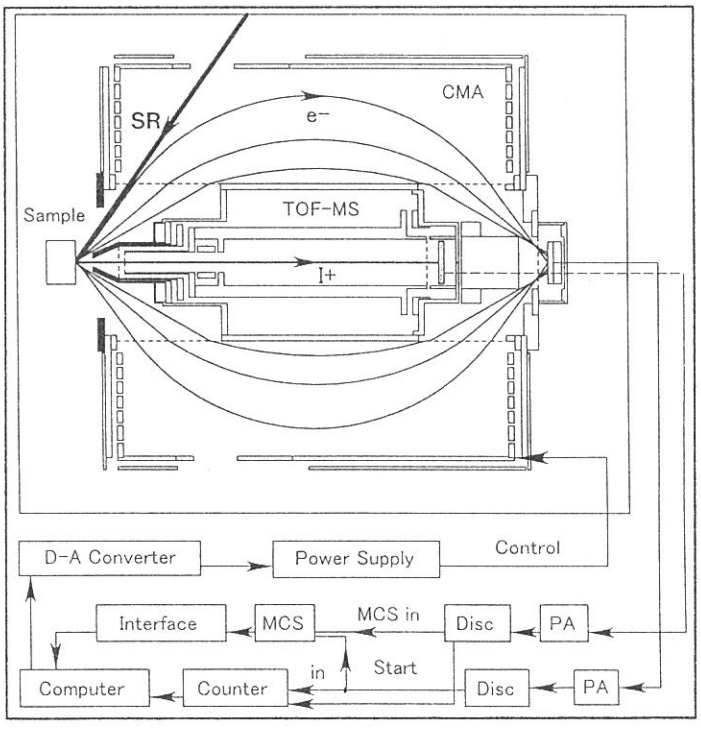

Figure 1. Schematic drawing of the third EICO apparatus.

References

[1] K. Mase *et al.*, *J. Electron Spectros. Relat. Phenom.* **101-103**, 13 (1999).

[2] K. Mase *et al.*, *Rev. Sci. Inst.* **68**, 1703 (1997).

[3] K. Mase *et al.*, *Surf. Sci.*, in press.

(BL2B2)

Performance of the Dragon-type monochromator

Masaki ONO[A], Hiroaki YOSHIDA[B], Hideo HATTORI[A] and Koichiro MITSUKE[A]

[A] *Department of VUV Photoscience, Institute for Molecular Science, Okazaki, 444-8585, Japan*
[B] *Department of Physical Science, Hiroshima University, Higashi-Hiroshima, 739-8526, Japan*

A Dragon-type monochromator has been newly constructed at the bending-magnet beamline BL2B2 of the UVSOR. The monochromator has been designed to cover the energy range of 20 – 200 eV with three gratings (G1 : 80 – 200 eV, G2 : 40 – 100 eV, G3 : 20 – 50 eV). A resolving power, $E/\Delta E$, of 5000 and a photon flux more than 1×10^{10} photons s^{-1} at 100 mA ring current are expected. The details of the monochromator were described in Ref. [1]. The optical alignment has been already finished. We have reported the performance of the monochromator, especially the resolving power and photon flux.

The resolving power has been evaluated from the ion yield spectra of the rare gas atoms ; the $3d_{5/2}^{-1}5p$ line of Kr (91.2 eV, exploited for G1 and G2) , $2snp + 2pns$ series of He (60 – 65 eV, for G2) and $3s^{-1}np$ series of Ar (25 – 30 eV, for G3). Figure 1 shows the ion yield spectrum of $3s^{-1}np$ series of Ar with a slit width of 100 μm. The series of the Rydberg states up to $n = 23$ is clearly observed. We have estimated the resolving power to be 12500 from the FWHM of the depression of $n = 18$ (2.3 meV) when the natural width, 0.23 meV calculated by n^{-3} rule, is ignored. The resolving power vs. slit width at 30 eV is shown in Figure 2. The solid line represent the dependence calculated theoretically by taking into account the entrance and exit slit widths, coma aberration and slope error of the grating [1]. The measured resolving power is higher than that expected.

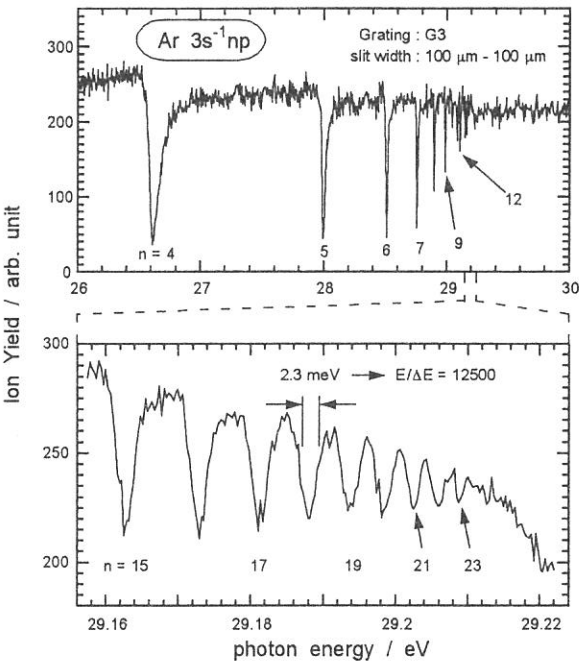

Fig. 1. Ion yield spectrum of $3s^{-1}np$ series of Ar with a slit width of 100 μm.

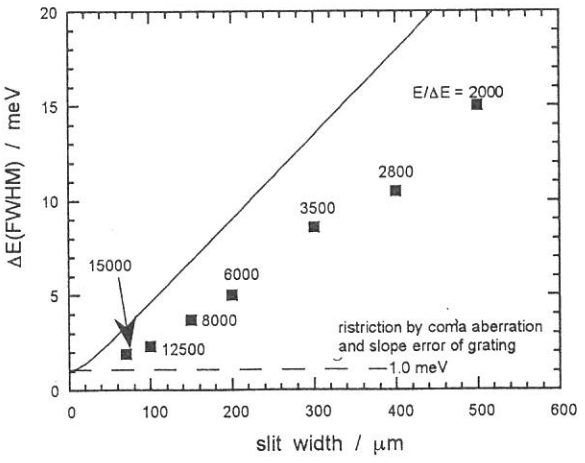

Fig. 2. Resolving power vs. slit width at 30 eV. The solid line shows the expected values [1].

The spectral shape of the $2snp + 2pns$ series of helium is asymmetric, and it is therefore difficult to estimate the resolution. However, the peaks become more symmetrical with increasing n because of the system resolution. Hence, we have judged the resolution based on the FWHM of the symmetrical peak. The resolution at 91.2 eV is obtained by fitting of the line shape of the $3d_{5/2}^{-1}5p$ peak of krypton to a Voigt function.

Figure 3 illustrates the resolving power and photon flux under the condition at the 100 mA ring current when both the entrance and exit slits are set to 100 μm wide. The solid line in the panel indicating the resolving power shows the expected values. Values of the resolving power measured at 30 eV and 60 eV are twice as high as those expected. It is lower than 5000 at 91.2 eV, though such performance has been predicted on the original design of the monochromator. At this energy the resolving power is also above the expected one. We have confirmation that the alignment procedure is fully completed.

The photon flux has been estimated by measuring the photocurrent of the gold mesh. The photon flux is more than 1×10^{10} photons s^{-1} in the region of 50 – 160 eV. In the region covered with G3 the photon flux seems to be low. However, the photon flux above 1×10^{10} photons s^{-1} has been achieved when the resolving power is lowered to 5000.

The alignment of the Dragon-type monochromator has been almost finished. The resolving power of 2000 – 8000 is available with the condition of the photon flux of 1×10^{10} photons s^{-1} at 100 mA ring current.

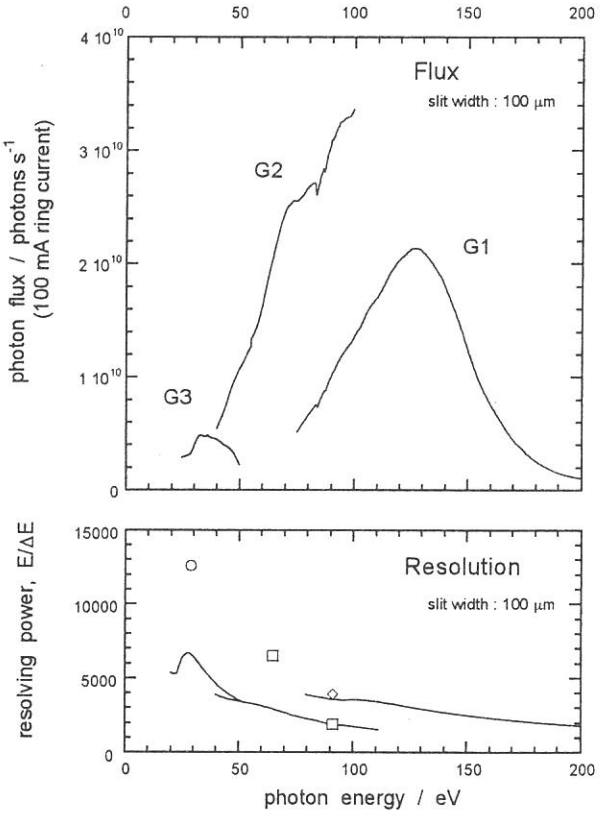

Fig. 3. Resolving power (down) and the photon flux at 100 mA ring current (up) when the entrance and exit slit widths are set to 100 μm. The solid lines in the lower panel show the expected values.

[1] H.Yoshida and K.Mitsuke, *J.Synchrotron Rad.* 5, (1998) 774.

(BL-4A)

Replacement of the new Pre-mirror Chamber in the beam line 4A

Harutaka Mekaru[a], Noritaka Takezoe[a], Hideyuki Noda[b], Hideaki Yanagita[c], Kazuhiro Kanda[d], Shinji Matsui[d], Kou Kurosawa[a], Eiken Nakamura[a], and Tsuneo Urisu[a]

[a]*Institute for Molecular Science, Okazaki, Aichi, 444-8585*
[b]*The Graduate University for Advanced Studies, Okazaki, Aichi, 444-8585*
[c]*Department of Electric and Electronic engineering, Miyazaki University, Miyazaki, Miyazaki 889-2192*
[d]*Laboratory of Advanced Science and Technology for Industry, Himeji Institute of Technology,, Ako, Hyogo 678-1201*

Since the beam line 4A1 and 4A2 are going to be used for experiments of fabricating nano-structures by SR-stimulated etching and thin film deposition, and for analysis of the SR-stimulated reaction by several *in situ* observation techniques, we established several criteria for the design of the beam lines. The beam spot size on the sample surface was designed to be $\geqq 3 \times 3$ mm^2. To obtain a large photon flux, we decided to use only one pre-mirror for focusing, designed so that it can accept as wide a horizontal divergence of the emitted beam from the light source as possible.

The pre-mirror of the beam line 4A1 is an elliptically-bent cylindrical quartz mirror with a Pt coating on its surface. (The radius of the cylindrical curvature is 253.0 mm and the longer and shorter radii of the elliptical curvature are, respectively, 4880 mm and 290 mm.) A length of the pre-mirror is 530 mm and a height is 30 mm. It was set at a point 2.35 m downstream from the light source point of the bending magnet with a grazing incident angle of 4 degrees. The horizontal and vertical acceptance angles of the pre-mirror are, respectively, 16.0 mrad and 13.0 mrad. The reflected beam is focused at a point 7.4 m downstream from the center of the pre-mirror and has an elliptical spot size of about 5 mm $\times$ 2 mm at this focus point.

The pre-mirror of the beam line 4A2 is also an elliptically-bent cylindrical quartz mirror with a Pt coating on its surface. (The radius of the cylindrical curvature is 210.0 mm and the longer and shorter radii of the elliptical curvature are, respectively, 7248 mm and 279 mm.) A length of the pre-mirror is 490 mm and a height is 30 mm. It was set at a point 2.35 m downstream from the light source point of the bending magnet with a grazing incident angle of 3 degrees. The horizontal and vertical acceptance angles of the pre-mirror are, respectively, 11.1 mrad and 13.0 mrad. The reflected beam is focused at a point 12.2 m downstream from the center of the pre-mirror.

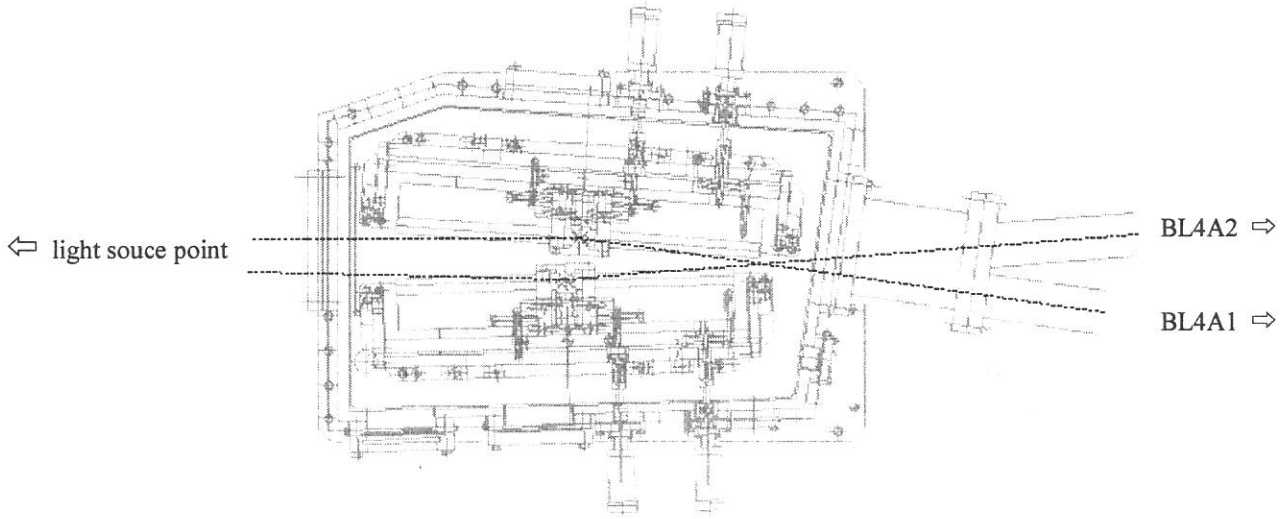

Figure 1. Top view of the pre-mirror chamber of the beam line 4A.

(BL8B1)

Improvement of the degree of liner-polarization at BL8B1

Tatsuo Gejo, Eiken Nakamura and Eiji Shigemasa
Institute for Molecular Science, Myodaiji, Okazaki 444-8585, Japan

It is well known that synchrotron radiation (SR) having a vertical spread of ~1 mrad from bending magnets is linearly polarized (more than 90%) horizontally. The degree of linear polarization depends on the detection angle for SR relative to the orbital plane of the electrons stored. This will be a maximum when the vertical position of the center of the first mirror matches with that of the orbital plane. At BL8B1 the degree of linear polarization was measured with the use of a soft X-ray multilayer polarizer and was determined to be about 0.6 [1]. This poor value was attributed to the fact that the vertical center of the acceptance angle of the first mirror was lower than the orbital plane.

The linear-polarization degree of monochromatized SR has been improved by the re-alignment of the beamline components (M1, M2, gratings, M3 and TOF chamber), with the help of well-polarized UV light. Fig. 1 shows the setup for monitoring the degree of linear polarization of the UV light. The vertical aperture of the diaphragm was placed in front of a UV filter and a polarizer. The width of the diaphragm was kept at 1mm during the measurements. In order to obtain only the central part of the photon beam, the polarization degree was monitored with the polarizer and a Si photodiode. Then, the position of the diaphragm was determined to be the polarization degree at maximum. After the determination of the central part of the SR beam, the heights of all the beamline components were moved so as to align the beam through the diaphragm. Consequently, we have moved them down 3mm to the ground level. The angle of the gratings was so important that a tilt angle of the monochromator was monitored during the re-alignment by a tilt sensor (Koku-Denshi MC100L) and was maintained at the fixed angle during the course of the experiments.

The improved polarization degree has been measured, again, by the soft X-ray multilayer polarizer and was determined to be more than 98%. This improvement will be particularly useful for Magnetic Circular Dichroism (MCD) measurements in core absorption.

Mr. Hayashi and Mr. Kondo at IMS deserve special thanks for their technical support. We are also indebted to Mr. Saito and Prof. Watanabe at Tohoku University for providing us the information on the degree of linear polarization.

[1] T. Hatano, W. Hu, M. Yamamoto and M. Watanabe, UVSOR Activity Report 1997, 64.

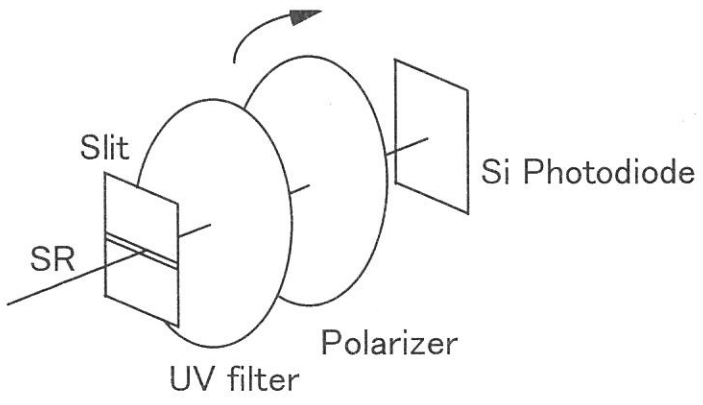

Fig. 1: The system for measurement of the polarization degree of UV light.

(BL4A2)

Design and Construction of BL-4A2 Beam Line for Nano-Structure Processing

N. Takezoe[1], H. Yanagida[1,2], K. Kurosawa[1], T. Urisu[1], H. Mekaru[1], H. Noda[3],
S. Matsui[4], K. Kanda[4] and H. Uchida[5]

[1]*Institute for molecular Science, Myodaiji, Okazaki, 444-8585, Japan*

[2]*Department of Electric and Electronic Engineering, Faculty of Engineering, Miyazaki University, Gakuenkibanadai-Nishi, Miyazaki, 889-2192, Japan*

[3]*The Graduate University for Advanced Studies, Myodaiji, Okazaki, 444-8585, Japan*

[4]*Laboratory of Advanced Science and Technology for Industry, Himeji Institute of Technology, Kamigori-cho, Ako-gun, Hyogo, 678-1205 Japan*

[5]*Electrical and Electronic Engineering, Toyohashi University of Technology, Tenpaku-cho, Toyohashi, 441-8580, Japan*

Nano structures must open new windows not only for surface physics and chemistry but also for electronic and photonic devices. Synchrotron radiation stimulated surface chemical reactions have been a most promising way to fabricate nano structures, because they offer a process with the advantages of high-site selectivity by core electron excitation and also free-of damage with atomic scale. Since a new beam line with higher flux is required for the processing, we have been designing and constructing BL-4A2 beam line for the nano structure fabrication.

We have been constructing a new beam line BL-4A2 which consists of white ray beam, ultra-high vacuum scanning tunneling microscope (UHV-STM) and photo-stimulated reaction chamber. In near future, we are going to join a near field optical microscope for monitoring optical properties with the atomic scale to them. Figure 1 shows the outline of the beam line, which consists of pre-focusing mirror (M1), secondary mirror (M2), monitor port, two differential pumping ports, reaction chamber and STM. An elliptically bent cylindrical mirror made of quartz coated with platinum is used as the pre-mirror. The reflected beam is focused at a point of 12.7 m down stream from the center of the pre-mirror and has a spot size of 8x6 mm^2. Low energy electron diffraction (LEED) is installed in the reaction chamber for in-situ characterization of substrate surfaces and also STM is for

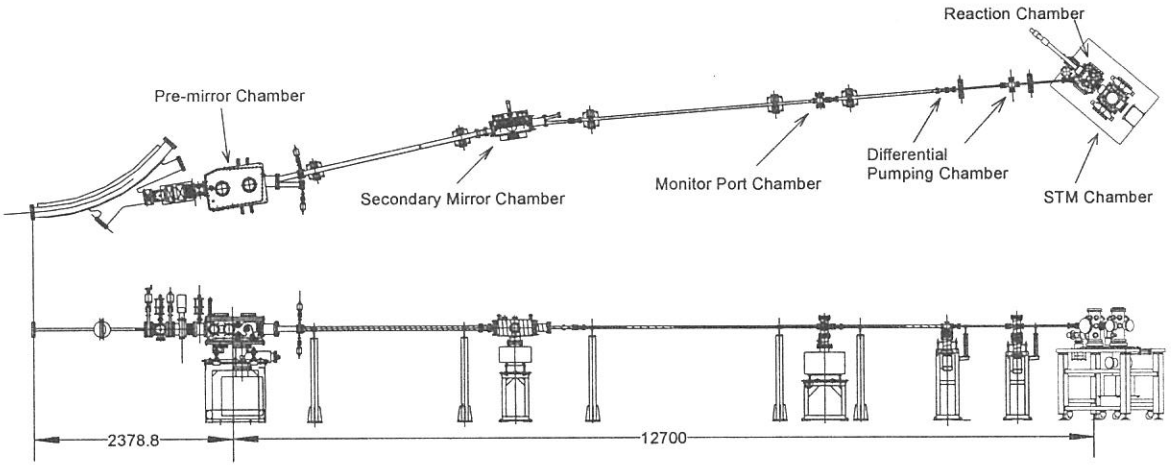

Figure 1. Schematic drawings of the BL-4A2 beam line with a reaction chamber and STM.

observation of the surface processes with atomic scale. We have a plan to make a photonic band-gap structures in a SiO_2 planer waveguide and study evanescent light from the waveguide surfaces with near field optical microscope.

First, we replaced the mirror chamber of the beam line BL4A with the new type of thing. In case of the new model chamber, when an optical-axis was considered a x-axis and a perpendicular on the floor was considered a z-axis, the tilting (ϕ) which moved around the x-axis, and a liner motion in the y-axis direction are possible. Though only the rotation which moved around the z-axis could be adjusted in case of the usual chamber by the liner motion feedthroughs in the vacuum. Helium neon laser was irradiated from the downstream side of the beam line to adjust the optical-axis, without SR. It is because the front-end valve has the atmosphere leak and it is dangerous to keep the pre-mirror chamber atmospheric pressure for a long time. Each degree of vacuum of the pre-mirror chamber and the secondary-mirror chamber reaches 9.8×10^{-10} Torr and 3×10^{-10} Torr at present. However, a mirror of a BL4A2 inside the pre-mirror chamber, which should be faced on the xy-plane, is slanted and it was proved that a beam form warped in the parallelogram. It can think that this is because a displacement occurred in the holder by the vibration when a HELICOFLEX of the pre-mirror chamber were secondary tightened. The pre-mirror chamber will atmosphere leak on that occasion, and alignment will be done with the SR because the valve exchange of the front end is done when it is shut down next time. Therefore, the adjustment of the STM2 chamber that is an end station is being made in the present. We must attain the ultra high vacuum of 10^{-11}Torr level to do in-situ observation with STM. Besides, because it had to get rid of mechanical vibrations, usual exhaust was reconsidered and improved as the figure 2. A sputter ion pump of 400 m^3/s, a non-evaporable getter pump and a nitrogenous trap are attached to the bottom part of the STM chamber, and a TMP(turbo molecular pump) of 300 l/s is attached to the top and the TMP of 50 l/s is connected in series. The sputter ion pump of 200 m^3/s is attached to the reaction chamber. A present degree of vacuum is 8×10^{-11} Torr though heating of the sample holder and nitrogenous cooling aren't being done. Therefore, it will reach the degree of a vacuum that it aims at while an experiment is being done.

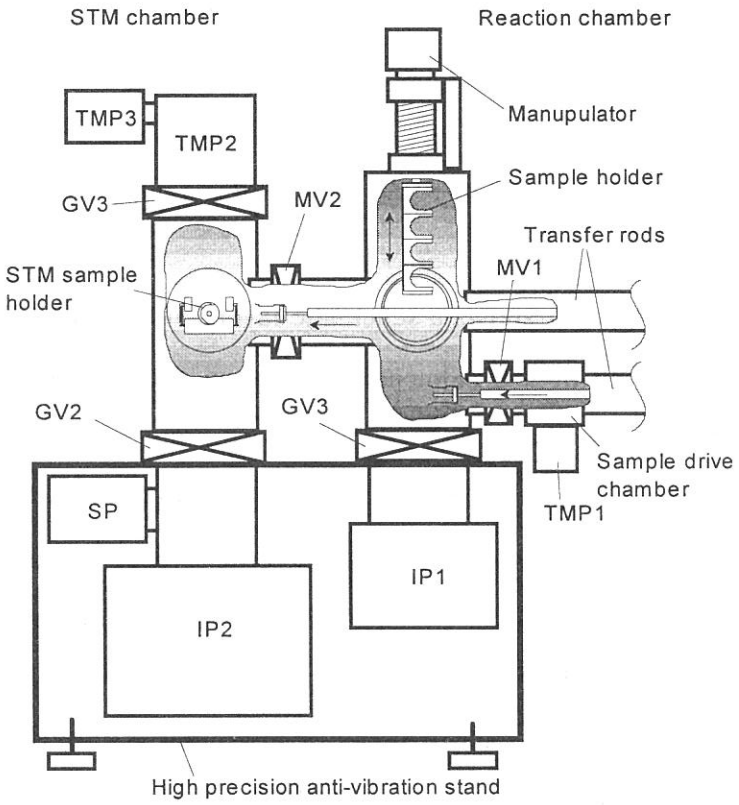

SP: Non-evaporable Getter Pump
GV1, 2, 3: Gate Valves
MV1, 2: Manual Gate Valves
TMP1, 2, 3: Turbo Molecular Pumps (1&3; 50 l/s, 2; 300 l/s)
IP1, 2: Sputter Ion Pumps (1; 0.2 m^3/s, 2; 0.4 m^3/s)

Figure 2. Schematic drawings of the improved exhaust system of the end-station.

(BL4B)

Design for a new monochromator on BL4B

Yasutaka Takata, Tatsuo Gejo, and Eiji Shigemasa
Institute for Molecular Science, Okazaki 444-8585, JAPAN

Recent conceptual and technological improvements to monochromators for synchrotron radiation have enabled us to realize various studies on vibrational spectroscopy in the soft x-ray range (100 ~ 1000 eV), which contains the *K*-shell thresholds of chemically important elements like C, N, and O, even without the use of undulator radiation [1]. At the UVSOR, there is only one monochromator for high resolution spectroscopy in the photon energy region of interest (250–550 eV). A maximum resolving power of 4000 at 400 eV is achievable with this monochromator, but due to a little complicated scanning mechanism, it has difficulty maintaining such high resolution in the entire photon energy range. Design study for a new monochromator at BL4B has recently been started in order to improve the situation. A Varied-line-spacing Plane Grating Monochromator (VPGM) has been chosen for this work. Thanks to the availability for high quality gratings and simple scanning mechanism, VPGM seems to be one of the most trustworthy monochromators to realizing high resolution in the soft x-ray range.

Figure 1 shows a schematic layout of the optical elements of the present VPGM. In front of all optical elements, there is an aperture, located 1.9 m from the source position. The usual setting of this aperture is 3.8 $mm_V \times 14.3$ mm_H, which limits the half acceptance angle to 1 $mrad_V \times 3.75$ $mrad_H$. The radiation is deflected horizontally by a cylindrical mirror M_0. This also serves as a vertical focusing mirror (sagittal focusing), which focuses the radiation onto an entrance slit S_1. A cylindrical mirror M_1 is located 1.1 m behind M_0, and focuses the radiation horizontally. M_0 and M_1 (Si substrates) are cooled from both sides by water-cooled copper blocks coated with Ni. A spherical mirror M_2 is one of the most important optical element to realizing high resolution, which focuses the radiation through S_1 onto an exit slit S_2. Two holographically ruled laminar profile plane gratings with the varied-line-spacing are designed to cover the energy range from 100 eV to 700 eV. The gratings with the groove densities of 266.7 and 800 l/mm cover the spectral ranges of 100–250 and 250–700 eV, and are interchangeable without breaking the vacuum. The

including angle of the gratings is 174°, and the fixed entrance- and exit-slit arm lengths are 4.0 and 4.006 m. A refocusing mirror M_3 has a toroidal shape, which focuses the monochromatized radiation at the sample position. The incidence angle of M_3 is 87.5°, in order to make the exit beam horizontal. All the gratings and mirrors are coated with Au.

The resolution of the present monochromator was studied by ray-tracing simulation as well as analytical estimation. As a result, it is found that a resolving power E/ΔE of more than 5000 is achievable over the energy range from 250 to 700 eV with one single grating having the groove density of 800 l/mm. It is also seen that the beam size (FWHM) at the sample position is smaller than 0.4 $mm_V \times 0.6$ mm_H, even with full size openings of the entrance and exit slits. The throughput photon flux estimated ranges from 10^8 to 10^{10} photons/sec for the ring current of 100 mA, with a resolving power of 5000.

References

[1] Y. Kitajima et al., J. Synchrotron Rad. **5**, 729 (1998).

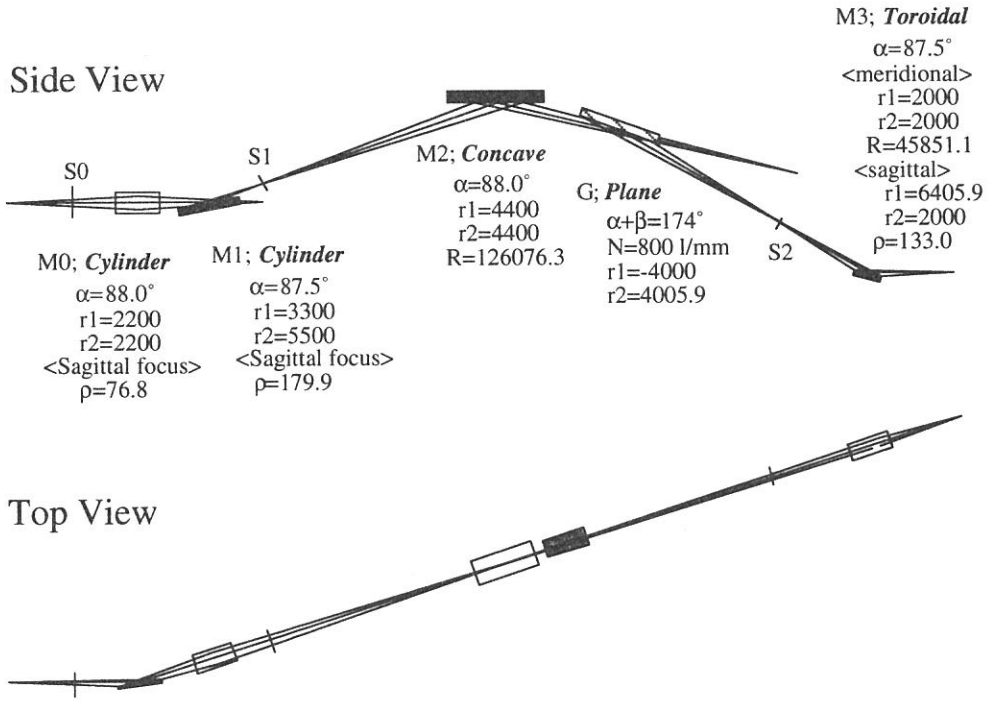

Figure 1. Schematic layout of the designed monochromator.

BL5B

Two-color reflection multilayers for He-I and He-II resonance lines for microUPS using Schwarzschild Objective

Takeo EJIMA, Yuzi KONDO, and Makoto WATANABE
Research Institute for Scientific Measurements, Tohoku University, 2-1-1 Katahira, Aoba-ku, Sendai, 980-8577

Two-color multilayers reflecting both He-I (58.4 nm) and He-II (30.4 nm) resonance lines have been designed and fabricated for reflection coatings of Schwarzschild objectives of micro ultraviolet photoelectron spectroscopy (UPS) instruments. They were designed to consist of top layers and piled double layers so that their reflectances for both He-I and He-II resonance lines are more than 20 %. Fabricated are multilayers of SiC(top layer)-Mg/SiC(double layers) and SiC(top layer)-Mg/Y_2O_3 (double layers), and their reflectances for the He-I and the He-II are 23 % and 17 %, and 20 % and 23 %, respectively.

KEYWORDS: multilayer, He-I, He-II, resonance line, ultraviolet, reflection coating, mirror

1. Introduction

Photoelectron micro-spectroscopy is powerful method to investigate electronic structures of condensed matters of small size and those consisting of grains.[1] In laboratories, He-I (58.4 nm) and He-II (30.4 nm) resonance lines are used for ultraviolet photoelectron spectroscopy (UPS). Changing the exciting photon energy for photoelectron spectroscopy is important to obtain partial density of states (p-DOS) of valence bands.[2] Even if the energies of the initial states are same, symmetries of final states excited by He-I and He-II lines are different. The difference is due to the dependence of the transition matrix element on the exciting photon energies.[2,3] Therefore, the p-DOS with different symmetries can be seen even if the photoelectrons are emitted from valence states with the same binding energy. For example, the Ce 4f p-DOS's in $CeSi_2$ were obtained using He-I and He-II lines.[4] Therefore, the microUPS instruments of the practical use are very promising tool if the suitable demagnifying optical elements for both resonance lines are available.

The Schwarzschild objective (SO) is one of microfocusing optical elements in ultraviolet and soft x-ray regions.[5] In the SO unit, the mirror surfaces should be coated with high reflectance materials for normal incidence. One of such materials is the multilayer of the piled double layers consisting of two materials with period of more than 10 (usual multilayer). However, the usual multilayer has a high reflectivity at only a certain wavelength for a fixed angle of incidence.

Therefore, in this paper, special *two-color* multilayers reflecting both He-I and He-II resonance lines have been designed and fabricated for reflection coatings of the SO units in microUPS instruments.

2. Design and fabrication of *two-color* multilayers

There are several materials which reflect He-I line efficiently (> 20 %) by their single layers. However, there are no such materials for He-II line, so that usual multilayers are required. Extinction coefficients of materials are generally larger for He-I line than for He-II line. Therefore, the *two-color* multilayer was designed to be composed of the top single layer reflecting He-I line with high transmittance for He-II line and the usual multilayer reflecting He-II line under the top layer.

To obtain high reflectance at interfaces, two materials were selected according to the following principle. The principle is that, the absolute value of the difference of Fresnel reflection coefficients (*abs.*) between two materials has to be as large as possible at the design wavelength.[6] (The Fresnel coefficient of the vacuum is 0.) Adding to this, the imaginary parts of these Fresnel coefficients (*im.*) which are proportional to the extinction coefficients have to be as small as possible to minimize the absorption of the light.

In Figs. 1(a) and 1(b), Fresnel reflection coefficients of various materials for He-I and He-II resonance lines at the angle of incidence of 0° are plotted in the complex-plane using the Henke's and the Palik's data.[7-9] The single layer of SiC was chosen for the He-I reflection, because in SiC the *abs.* is large for He-I line as shown in Fig. 1(a), and the *im.* is small for He-II line as shown in Fig. 1(b). The piled double layers of Mg/Y_2O_3 and Mg/SiC were chosen for the He-II reflection. In the case of Mg/Y_2O_3 multilayer, the *abs.* between Mg and Y_2O_3 is large as shown in Fig. 1(b), so that the high reflectance can be achieved by a small number of layers. In the case of Mg/SiC multilayer, the *abs.* between Mg and SiC is small, but the *im.* of each material is small, so that the high reflectance can be achieved by a large number of layers.

Calculations of reflectance of the multilayers are performed using the recurrent method with extension as for the number of materials.[6] The *two-color* multilayers were designed to have reflectances of more than 20 % for both He-I and He-II lines. Through the calculations, the thickness of the layers in the SiC (top layer)-Mg/SiC (double layers) and the SiC (top layer)-Mg/Y_2O_3 (double layers) were determined. The former multilayer has an advantage of being composed of only two materials. Calculated reflectances are presented as dashed curves in figure 2. The angle of incidence to all multilayers is 10° in the figure.

All samples were fabricated by magnetron sputtering. The sputtering system (ANELVA SPL-500) is of a vertical type with the targets and substrates placed vertically. Mg was dc-sputtered with an input power of 100 W, and SiC and Y_2O_3 were rf-sputtered with input power of 200 W. The Ar pressure was 2.0 mTorr for all the depositions, while the base pressure was 2.0×10^{-6} Torr. The multilayers were deposited onto commercially avail-

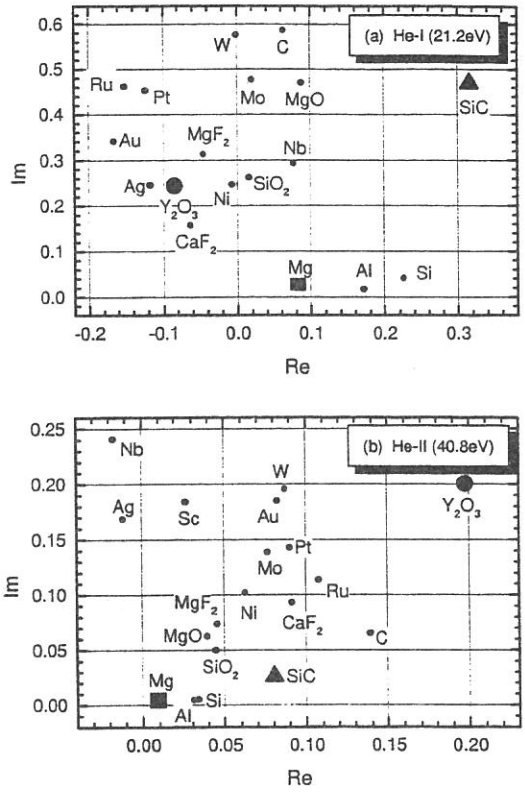

Fig.1: Fresnel reflection coefficients of various materials for He-I (58.4 nm), (a), and He-II (30.4 nm) resonance lines, (b).

able 4 inch (10.16 cm) Si wafers. Effective deposition rate of Mg, SiC, and Y_2O_3 are 0.12 nm/s, 0.02 nm/s, and 0.04 nm/s, respectively. The film thickness was measured by an x-ray diffractometer within 5 % error for the top layers and 2 % error for the double layers.

3. Results and Discussion

Reflectances of *two-color* multilayers were measured with a reflectometer at the beamline BL5B.[10] In this experiments, we used the combinations of the G3 grating and the M25 mirror for the 25–60 nm range and the G3 grating and the M26 mirror for the 50–70 nm range. An average resolving power $\lambda/d\lambda$ was about 500. The resolution of the angle of incidence was about 1° in reflection measurements.

In Fig. 2, reflectances of SiC(14.4 nm)-Mg(10.4 nm)/SiC(6.1 nm) multilayer at the angle of incidence of 10° are presented. In the figure, the left and right solid curves represent experimental results obtained by the G3-M25 and G3-M26 combinations, respectively. The dashed curve represents the calculated result. In the figure, the measured reflectance shows the rise around 28 nm, becomes maximum (20 %) at 31 nm and decreases toward 33 nm. From 33 nm to 40 nm, the reflectance is less than 10 % showing small oscillation. Above 40 nm, the reflectance increases toward the longer wavelength. Comparing experimental result obtained by G3-M25 combination with calculated ones, spectral shapes and absolute values of reflectances resemble to each other between 30 nm and 40 nm. The measured reflectance obtained by the G3-M25 combination did not connect smoothly to that obtained by the G3-M26 combination between 50 nm and 60 nm. The reflectance obtained by G3-M26 combination increases from 20 % to 30 % as the wavelength increases from 50 nm to 70 nm. The measured reflectance obtained by G3-M26 does not differ much with the calculated one above 55 nm. Therefore, we supposed the discrepancy may be due to the effect of the higher order light in the output light in the G3-M25 combination. Therefore, we adopted the results of the G3-M26 combination as the obtained values of the reflectances for He-I line. The reflectance of the SiC-Mg/SiC for the He-I is 23 % and for the He-II, 17 %.

In this study, the reflectance of the SiC-Mg/Y_2O_3 was also measured. It was 20 % for the He-I and 23 % for the He-II. The detailed results will be reported elsewhere.

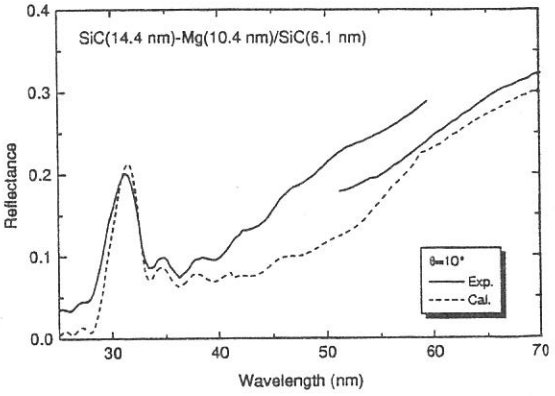

Fig.2: Measured reflectance of SiC-Mg/SiC multilayers for 10° angle of incidence.

References

1) *see for instance,* H. W. Ade: Nucl. Instrum. Methods Phys. Res. **A319** (1992) 311.
2) *Photoemission in Solids I*, ed. M. Cardona and L. Ley, (New York, Springer-Verlag, 1978).
3) J. J. Yeh and I. Lindau: At. Data Nucl. Data Tables **32** (1985) 1.
4) M. Grioni, D. Malterre, P. Weibel, B. Dordel and Y. Baer: Physica **B 38–43** (1993) 186.
5) see for instance, F. Cerrina: J. Imag. Sci. **30** (1986) 80.
6) M. Yamamoto, S. Nakayama and T. Namioka: SPIE Vol. **984** (1988) 160.
7) *Handbook of Optical Constants of Solids*, ed. E. D. Palik, (San Diego, Acad. Press. Inc., 1985).
8) B. L. Henke, P. Lee, T. J. Tanaka, R. L. Shimabukuro and B. K. Fujikawa: At. Data Nucl. Data Tables **27** (1985) 1.
9) B. L. Henke, J. C. Davis, E. M. Gullikson and R. C. C. Perera: Lawrence Berkley Laboratory **LBL-26259** and a diskette containing the data (1988).
10) M. Sakurai, S. Morita, J. Fujita, H. Yonezu, K. Fukui, K. Sakai, E. Nakamura, M. Watanabe, E. Ishiguro and K. Yamashita: Rev. Sci. Instrum. **60** (1989) 2089.

(BL5B)

On the diminishment of the high order light in the extreme ultraviolet region

*M.Nakamura, *A.Yamazaki, *K.Shiomi, and #I.Yoshikawa

* *Faculty of Earth and Planetary Science, University of Tokyo, Bunkyo-ku, Tokyo 113-0033*

\# *Institute of Space and Astronautical Science, Sagamihara, Kanagawa 229-8510*

We plan to optically observe ion and neutral atom distributions in space plasma environment. Ions and atoms resonantly scatter the solar emissions in extreme ultraviolet region. Our targets are helium ion emission at 30.4nm (HeII emission), helium atom 58.4nm (HeI emission) and oxygen ion 83.4nm (OII emission). Intensity of emission is proportional to column density of particles along the line of the sight, so optical observations bring to us the macroscopic particle distribution.

Japan's Mars orbiter Planet-B (NOZOMI) was launched in July 1998 to the parking orbit around the earth and now is cruising to the Mars orbiter. The eXtreme UltraViolet (XUV) scanner is onboard the NOZOMI spacecraft and observes resonantly scattered light from helium atoms and ions. We succeeded to observe the terrestrial plasmasphere by detecting HeII emission [1] and the emission reflected from the surface of the moon on the parking orbit, and in the cruising phase to the Mars detect HeI and HeII emission from the interplanetary medium.

Also we are developing a mirror for detecting OII emission. In this machine time, we examine the characteristics of SOR beam at BL-5B and build the method to produce monochromic beam, which includes no high order light in extreme ultraviolet region, especially from 20nm to 100nm of wavelength. Finally, we measure transmittance of thin metal filters, reflectivity of multilayer-coated mirrors and quantum efficiency of Micro Channel Plates (MCPs) detector with the monochromic beam.

Method to produce monochromic light.

In the latest machine time, we confirm that an Al/Mg/Al filter removes the high order light in 25-50nm wavelength region and make the monochromic light beam produced to the calibration chamber. As the same way, we tried to remove high order light in other region with Al 430.6nm-thickness filter, Sn 354.5nm filter, and In 583.0nm filter. Figure 1 shows diffraction patterns of beams transmitting the Sn filter at the wavelength of 58.4nm. This pattern has no high order line, therefore, it is clear that the beams consist of one specific wavelength light. Furthermore we measure transmittances of some metal filers and compare the ones evaluated with discharged light source. The results are shown as Figure 2a, 2b, and 2c, which represent the transmittance of Al 149.2nm, Sn 184.0nm, and In 158.0nm filter, respectively. We conclude that high order cut filter have good performance.

Quantum efficiency of MCPs

The quantum efficiency measurement of backup MCPs for the XUV is effective to estimate

temporal development of the detectable efficiency on flight. So we revalue quantum efficiency of a reference MCPs for laboratory at 30.4nm and 58.4nm. We evaluate the efficiency by the comparison between the output current from absolutely calibrated photodiode and the count rate of the MCPs, to be 5% at 58.4nm and 10% at 30.4nm.

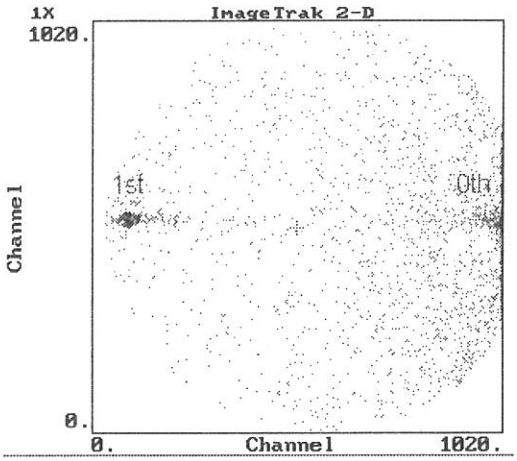

Figure 1. The diffraction pattern of 584nm light through Sn filter.

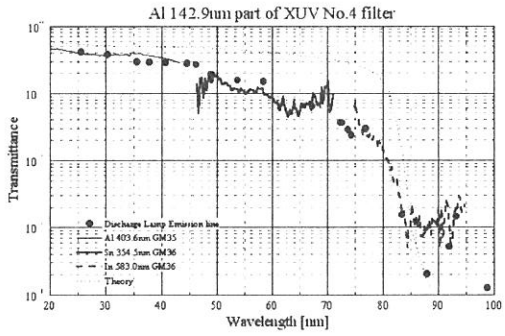

Figure 2a. The transmittance of Al filter.

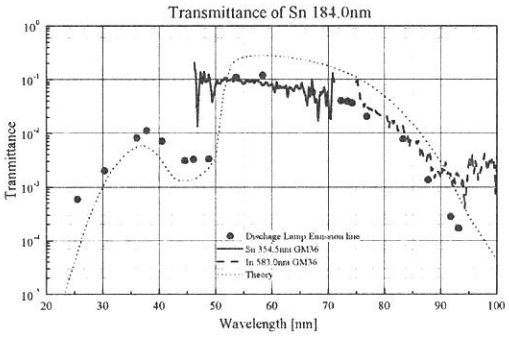

Figure 2b. The transmittance of Sn filter.

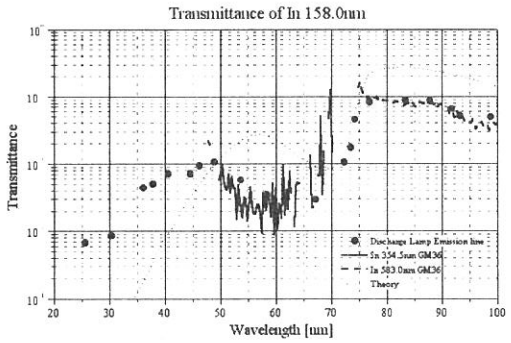

Figure 2c. The transmittance of In Filter

Reference

[1] Nakamura,M., I.Yoshikawa, A.Yamazaki, K.Shiomi, Y.Takizawa, M.Hirahara, K.Yamashita, Y.Saito, and W.Miyake, Terrestrial Plasmaspheric Imaging by an Extreme Ultraviolet Scanner on Planet-B, *Geophys. Res. Lett., 27,* 141, 2000.

(BL5B)

Contrast Measurement of Reflection Mask for Extreme Ultraviolet Lithography

Masahito Niibe, Takeo Watanabe, Hajime Nii, Takeshi Tanaka and Hiroo Kinoshita

Laboratory of Advanced Science &Technology for Iudustry, Himeji Institute of Technology,

3-1-2 Koto, Kamigoori, Ako-gun, Hyogo 678-1205 Japan

Extreme Ultraviolet Lithography (EUVL) is attracting much interest and actively studied as a new technology to fabricate semiconductor devices in near future generations. In the EUVL method, multilayer mirrors are used not only in the demagnifying projection optical system but also in the reflection masks to print IC patterns on wafers. The reflection masks have currently been developed for the wavelength of 13.5 nm and have been prepared by patterning metal thin films as absorber materials deposited on EUV reflecting substrates coated by Mo/Si multilayers. Although Au, Ge, W, and Ni have been used as a absorber metal previously, the studies on absorber materials and their processing method are insufficient.

We chose chromium, Cr, and tantalum, Ta, metals as a new absorbing material for EUVL reflection mask. These metals are frequently used in photomask or X-ray mask for lithography and their fabrication processes are well investigated. Figure 1 shows the calculated transmittance of EUV light for various metals at the wavelength of 13.5 nm. As shown in Fig. 1, the transmittance (or absorbing ability) of Cr and Ta metals for the EUV light is nearly equal to that of tungsten, W.

We have fabricated the reflection masks with Cr or Ta metal absorbers deposited on top of Mo/Si multilayer reflectors. The Cr absorber mask with absorbing film thickness of 44 nm was patterned by conventional lift-off technique. The schematic diagram of the fabrication process of Ta absorber mask is shown in Fig. 2. The Ta absorbing layer with 100 nm thickness was deposited on top of the multilayer with 10-nm-thickness SiO2 etch-stop layer. The Ta absorber mask was patterned by ECR-plasma etching technique.

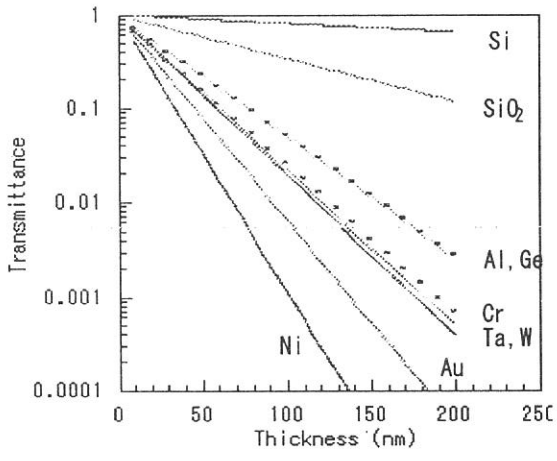

Fig. 1. Transmittance of metals at the wavelength of 13.5 nm.

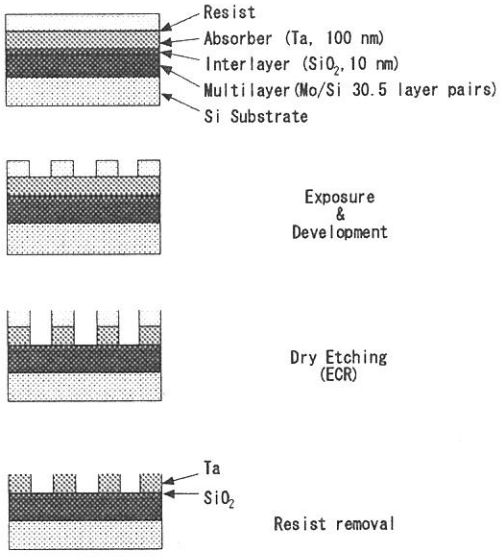

Fig. 2. Fabrication process of Ta absorber reflection mask

The mask contrast measurement was carried out by synchrotron radiation source beamline with plane-grating monochromater around the wavelength of 13.5 nm (UVSOR BL-5B). A silicon membrane with thickness of 150 nm was used as a low-pass filter. In the mask with 3" Si wafer substrate, we made a reflectivity measurement pattern of 4 mm square in addition to resolution evaluation patterns illustrated in Fig. 3. The contrast was measured by measuring the reflectivity of reflecting and absorbing parts of the patterns using movable stage in the reflectivity measurement system.

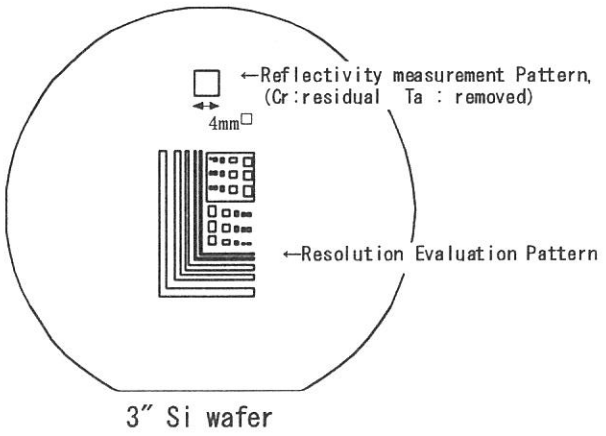

Fig. 3. Mask patterns of the present study

The peak reflectivity of the non-processed surface of Mo/Si multilayer deposited by a RF-magnetron sputtering method was about 62%. For the Cr absorber (44 nm thickness) mask, measured peak reflectivities at the reflecting and absorbing parts of the processed patterns were about 59% and 4.9%, respectively. The reflection contrast of the Cr absorber mask was about 12. On the other hand for the Ta absorber (100 nm thickness) mask, measured peak reflectivities at the reflecting and absorbing parts of the processed patterns were about 50% and 0.48%, respectively. The reflection contrast was about 105. From an AFM observation we got a roughness value of 1.3 nm(rms) on the surface of SiO2 etch-stop layer of the Ta absorber mask. The reduction of the peak reflectivity at the reflecting part of Ta absorber mask would be coursed by both absorption and scattering of light by SiO2 etch-stop layer.

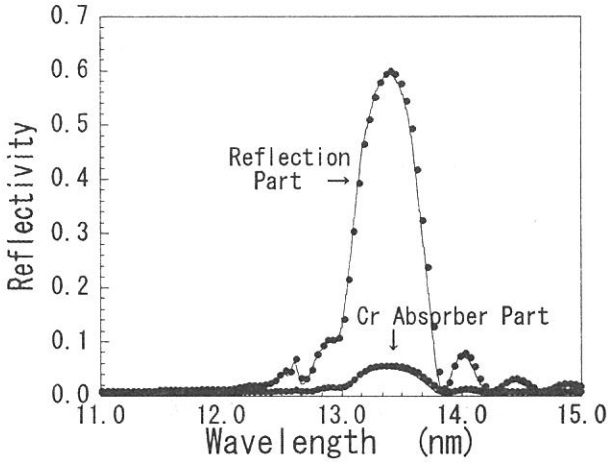

Fig. 4. Reflectivity of the Cr absorber reflection mask

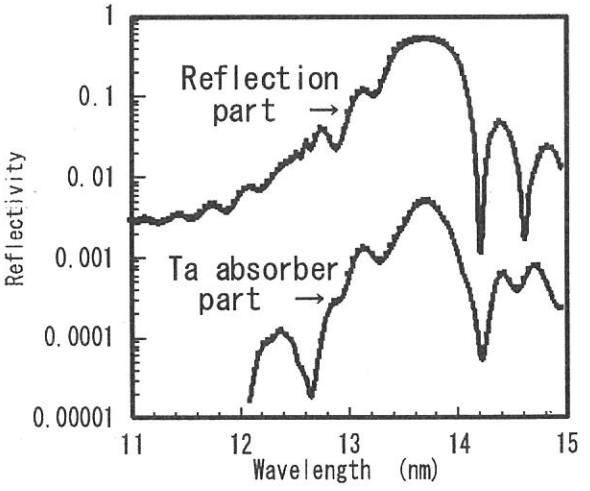

Fig. 5. Reflectivity of the Ta absorber reflection mask

It is noted that the masks were prepared at about one year before the reflectivity measurements and had been kept in the normal air. However there was no significant degradation of the reflectance or surface quality of the reflection masks.

(BL7A)

Performance of KTP monochromator crystals

Eiji Shigemasa
UVSOR, Institute for Molecular Science, Okazaki 444-8585, JAPAN

A variety of monochromator crystals with different 2d spacings is required for providing the monochromatized radiation in the soft x-ray region (0.7–3.5 keV) with double-crystal monochromators. Above about 1.7 keV, semiconductor crystals such as InSb and Si are available and it is known that such crystals are thermally strong and can endure long exposure to the intense X-rays even from the 4T wiggler , which is installed in the straight section upstream of the B7 bending magnet. Below this energy, the Al (~1550 eV) and Mg (~1300 eV) *K*-edges lie. It had been necessary to use beryl and quartz crystals to approach these two edges. However, these crystals are quite sensitive to radiation damage with considerable degradation in performance. Furthermore, the beryl and quartz crystals contain the Al and Si elements, respectively. This property prevent users from performing EXAFS measurements at the Mg and Al *K*-edges.

The combination of an artificial crystal, YB_{66}(400), with the wiggler has been another possibility to access the Al and Mg *K*-edges at BL7A in the past [1]. Their low reflectivity makes YB_{66} unsuitable for the radiation from the bending magnet. The focusing mirror system for the wiggler radiation was successfully installed in 1998 [2]. The basic ability to cover the Mg, Al, and Si *K*-edges with a single pair of monochromator crystals is very fascinating, but there is a disadvantageous property for the EXAFS experiments with the YB_{66} crystals, that is, two positive glitches at 1385 and 1438 eV caused by anomalous scattering for the (600) reflection at the Y L_{III} (2080eV) and L_{II} (2156eV) edges. It is quite hard to compensate the glitches completely even though the cutoff mirror is introduced.

In order to meet the demand to perform the EXAFS experiments at the Mg and Al *K*-edges in the UVSOR, a pair of $KTiOPO_4$(011) (KTP) crystals has been introduced and its performance test has been carried out on BL7A and BL1A. Figure 1 shows the photon intensity of the KTP monochromator crystals over the photon energy range 1200–3000 eV, comparing with those from other crystals. The silicon photodiode from IRD Co. was used to estimate the photon flux for each pair of crystals. The solid line represents the photon flux

for the KTP crystals measured after the optimization at 1500 eV, and the solid line with black circles indicates that the intensity was measured at each data point showed by the circles after the optimization. Comparing with these two curves, it is clear that the detuning by the irradiation happens, even against the radiation from the bending magnet. However, it can easily be seen that the photon flux from the KTP crystals without the use of the wiggler radiation is almost the same as that from the YB_{66} crystals combined with the wiggler and the focusing mirror system. The weak structure around 1800 eV and sharp drop around 2150 eV on the curve corresponding to the KTP crystals are attributed to the Si *K*-edge jump of the photodiode and to the P *K*-edge absorption of the KTP crystals, respectively. The excellent ability to cover the Mg, Al, and Si *K*-edges without any structures is quite suitable for performing the EXAFS measurements at the Mg and Al *K*-edges.

References

[1] T. Kinoshita et al., UVSOR Activity Report 1997, p. 62.
[2] T. Kinoshita et al., UVSOR Activity Report 1998, p. 41.

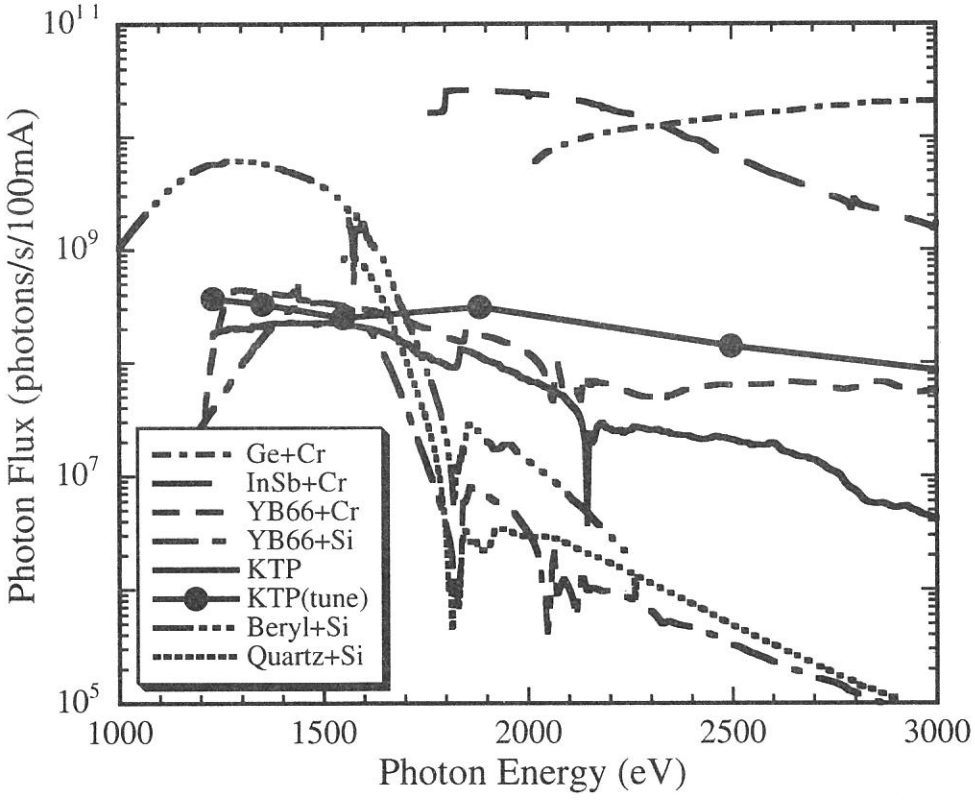

Figure 1. Throughput from KTP monochromator crystals on BL7A, in comparison with those for several combinations of the focussing mirrors and the monochromator crystals. Except for KTP, the 4T wiggler radiation was used as a light source.

(BL7B)

Present Performance of BL7B 3m Normal Incidence Monochromator

Kazutoshi FUKUI, Hiroshi MIURA[1], Hideyuki NAKAGAWA[1], Iwao SHIMOYAMA[2],
Kazumichi NAKAGAWA[3], Hidekazu OKAMURA[4], Takao NAMBA[4],
Masami HASUMOTO and Toyohiko KINOSHITA[5]

Institute for Molecular Science, Okazaki 444-8585, Japan

Fax +81-564-54-7079, fukui@ims.ac.jp

[1] *Faculty of Engineering, Fukui University, Fukui 910-8507, Japan*

[2] *Japan Atomic energy Research Institute, Ibaraki 319-1195, Japan*

[3] *Faculty of Human Development, Kobe University, Kobe 657-8501, Japan*

[4] *Faculty of Science, Kobe University, Kobe 657-8501, Japan*

[5] *SRL-ISSP, University of Tokyo, KEK-PF, Tsukuba 305-0801, Japan*

The beamline BL7B at the UVSOR facility for solid-state spectroscopy has been opening for users from April 1999. This beamline is reconstructed on the basis that the synchrotron radiation is still an important light source, not only for the VUV region but also for the UV, VIS and IR regions, owing to the wavelength continuity of synchrotron radiation with no structure. Then, this 3 m normal incidence monochromator (modified version of McPherson model 2253) covers the 50 – 1000 nm range with three gratings. The optical design and setup has been reported in Ref. 1.

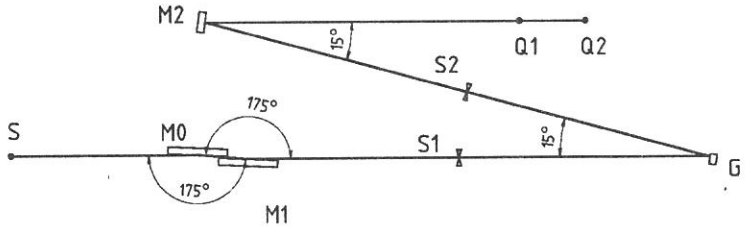

Fig. 1

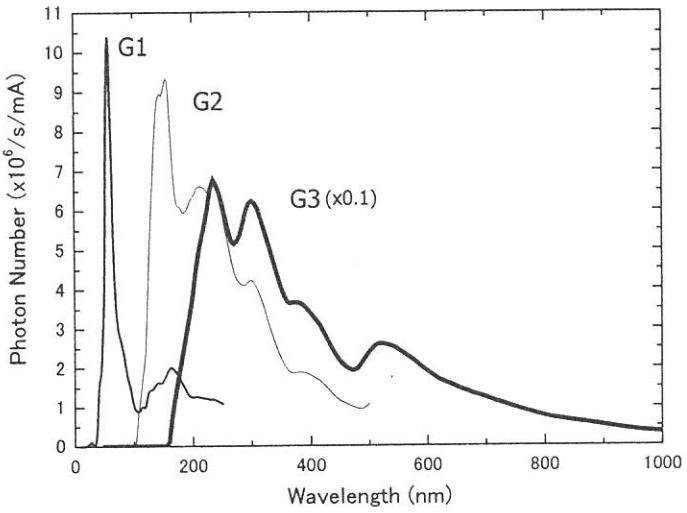

Fig. 2

The outline of the new beamline is illustrated at BL7B page of Status of UVSOR in this report. The optical design is also shown in Fig. 1. The design parameters of the optical elements are summarized in Table 1, 2 and 3 in Ref. 2 without coating material of G2 as mentioned after. The coverange of the three gratings in design is

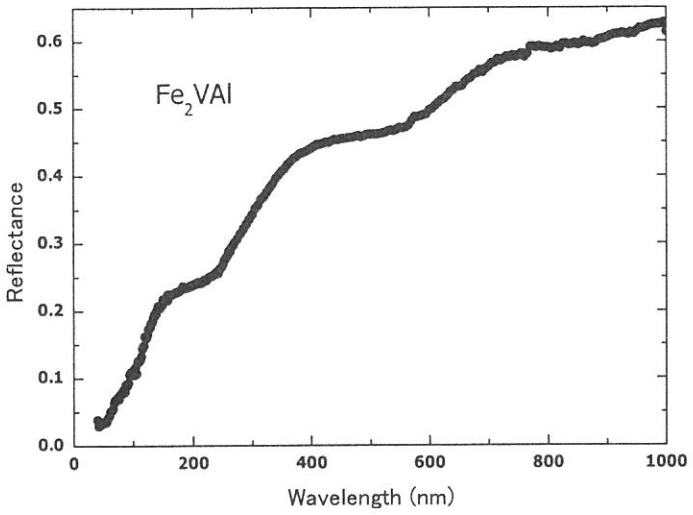

Fig. 3

50 – 150 nm for G1, 80 – 300 nm for G2 and 150 – 1000 nm for G3. This beamline covers the wide wavelength range, so that the reduction of the higher order light becomes important. Good purity of the monochromated light is almost fulfilled over whole wavelength by using the low wavelength cut filters such as LiF, quartz, pyrex glass and colored glasses.

Figure 2 shows the output spectra of BL7B. Both entrance and exit slits are 50μm. LiF and quartz filters are used in G2 and G3 spectra, respectively. Re-coating from Al to Au of G2 gives us the sufficient flux increase at higher energy of G2 region. It is difficult to estimate the intensity of the scattered light, but comparison between the spectra with and without the filters represents that the intensity ratio of the visible scattered light to the average output is expected less than 0.5%. Figure 3 shows Fe_2VAl reflectance spectrum as an example of the wide range measurements. Details of the spectrum will be seen in Ref.3.

References

[1] K. Fukui, H. Nakagawa, I. Shimoyama, K. Nakagawa, H. Okamura, T. Nanba, M. Hasumoto and T. Kinoshita, J. Synchrotron Rad. 5 (1998) 836.

[2] K. Fukui, H. Nakagawa, I. Shimoyama, K. Nakagawa, H. Okamura, T. Nanba, M. Hasumoto and T. Kinoshita, UVSOR Activity Reprot 1998, 1999, p. 42.

[3] H. Okamura, J. Kawahara, T. Nanba, S. Kimura, K. Soda, U. Mizutani, Y. Nishino, M. Kato, I. Shimoyama, H. Miura, K. Fukui, K. Nakagawa, H. Nakagawa, T. Kinoshita, Phys. Rev. Lett., in press.